

FATIGUE PERFORMANCE AND CYCLIC DEFORMATION BEHAVIOUR OF TITANIUM TI-6AL-4V ADDITIVELY MANUFACTURED BY w-DED

R. Plaskitt¹, M. Hill¹, A. K. Syed², X. Zhang²

¹ Hottinger Bruel & Kjaer Ltd, United Kingdom, rob.plaskitt@hbkworld.com

² Coventry University, United Kingdom

Abstract: Metal additive manufacturing (AM) has rapidly come to prominence as a valid and convenient alternative to other production techniques. There is a growing body of evidence to realise its advantages in terms of lead-time reduction; increased design flexibility and capability; and reduced manufacturing cost, energy and waste. Metal AM techniques can be categorised based upon the form of the material they use (powder or wire), the heat source (laser beam, electron beam, electric arc), or the way the material is delivered (pre-placed bed, or direct feed). Each of the metal AM technologies, given its particular properties, is best suited for specific applications. For example, in powder bed fusion (PBF) processes the selective melting of a pre-placed powder yields precise, net-shape components that can be very complex in design. However, their size is limited, cost is high, and material deposition build rates are low. In contrast, directed energy deposition (DED) processes can build near-net-shape parts, at many kilograms per hour, and with potentially no limitation to a components' size.

An important requirement for metal AM materials is to understand and quantify their performance under cyclic loading. This is necessary to satisfy the structural integrity of load-bearing AM structures, often safety-critical structures, for their damage tolerance, and their overall durability and reliability. This paper studies the performance under cyclic loading of ASTM Grade 5 titanium alloy Ti-6Al-4V (Ti64) manufactured by the w-DED process Wire + Arc Additive Manufacturing (WAAM).

WAAM Ti64 material was deposited from which test specimens were extracted for microstructure examination, and tensile and strain controlled fatigue tests conducted to understand the role of microstructure on monotonic and cyclic stress-strain response.

Keywords: cyclic deformation; low cycle fatigue; strain controlled fatigue test; titanium alloys; wire+arc additive manufacturing

BACKGROUND

The work reported here is a part of the New Wire Additive Manufacturing (NEWAM) research programme funded by the UK EPSRC Research Council (Grant No. EP/R027218/1) [1, 2]. The abstract for this paper includes the relevant summary from this grant application. This is a six year research programme (2018 to 2024) comprising four UK universities (Cranfield U., U. of Manchester, U. of Strathclyde, and Coventry U.), supported by industrial partners, including several from the aerospace industry. This NEWAM research programme is focused on the process, material and structural integrity of structures additively manufactured by wire based directed energy deposition w-DED (also known as

w-DEDAM), and particularly by the Wire + Arc Additive Manufacturing (WAAM) process, with research areas including:

- Process development
- Process modelling
- Process monitoring
- Non-destructive testing
- Material development
- Material modelling
- Material performance
- Structural integrity

Coventry University are leading these NEWAM material performance and structural integrity research areas to investigate material behaviour for:

- fatigue initiation – microstructure, defects, fatigue testing, characterisation & modelling
- fatigue fracture – damage tolerance, crack growth testing, characterisation & modelling
- residual stress – contour and diffraction test methods, residual stress intensity, modelling

Hottinger Bruel & Kjaer (HBK) are providing strain controlled fatigue testing and characterisation services to support this Coventry University fatigue initiation research. This paper is a summary of the authors' recent International Journal of Fatigue paper [3], and preliminary work presented at ESIAM 2021 [4] and HBK Technology Days 2021 [5]. The Syed et al journal paper [3] is more comprehensively referenced than is appropriate to include in this summary paper. The NEWAM structural integrity research is introduced by Zhang in [5], and the overall goals and business drivers introduced by Williams in [5]. The whole NEWAM research programme is reported on the NEWAM website (<https://newam.uk/>) and in research papers at <https://newam.uk/documents/research-papers/view> [6].

INTRODUCTION

Metallurgy and microstructure.

It is useful to briefly introduce some metallurgy and microstructure terminology though this is necessarily simplified and cannot include all the microstructure features described later. Unalloyed titanium is allotropic (exists in two or more forms), with an alpha ' α ' phase with a close packed hexagonal crystal structure changing to a beta ' β ' phase with a body centred cubic structure at about 900 °C. Cooling from the β phase transitions through a wide $\alpha+\beta$ transformation phase to an α phase. The cooling rate dictates the microstructure features formed, the size of the α colony (a group of α crystal structures) and the width of the α lath (seen as narrow parallel features). These can form as 'long' continuous α colonies or 'short' discontinuous α colonies. If the cooling rate is fast enough α nucleates inside prior β grains forming basketweave crystal structures, and if quenched the β phase transforms into a martensite α , with either hexagonal α' or orthorhombic α'' crystal structure. The distribution of crystallographic orientation of α and β crystal structures is described as 'texture', where no distinct texture indicates random orientation, and weak, moderate or strong texture indicates increasingly aligned crystal orientation. Material composed of different constituents, like these α and β phases, are described as heterogeneous.

The Ti-6Al-4V alloy is designed, with specific weight aluminium (6 wt%) and vanadium (4 wt%) alloying elements, for high fracture toughness and resistance to corrosion. The α phase is stabilised by the aluminium alloying element and the β phase is stabilised by the vanadium. Heat treatment by stress-relieving, β annealing, aging or solution treatment, changes the α and β microstructure to develop desirable mechanical properties. In summary Ti64 is a heat treatable alpha-beta titanium alloy whose α and β phase microstructure significantly influences macro mechanical properties including strength, ductility, fatigue, and fracture toughness.

In [3] Syed et al introduce important considerations for understanding Ti64 fatigue and cyclic behaviour from research of Ti64 additively manufactured by PBF processes.

1. Internal defects. The presence of PBF process inherent macroscopic defects that act as internal stress raisers leading to fatigue crack initiation and premature failure. Post-deposition heat

treatments such as hot isostatic pressing (HIPing) can improve the fatigue performance by reducing the size and population of these defects.

2. Cyclic stress-strain response. Cyclic softening behaviour where increasing strain amplitude causes greater elastic modulus reduction during cyclic loading and greater cyclic softening.
3. Microstructure. The shape, size and distribution of the α and β phases, grain boundaries, α colony size and α lath width. In laser-beam PBF Ti64 higher cyclic yield strength than wrought equivalent is due to the presence of α' martensite in as-built and finer α laths in stress relieved and β -annealed conditions. In electron-beam PBF Ti64 in an as-built and HIPed condition, with the loading axis parallel to the primary columnar β grain boundaries, the cyclic stress-strain response influences the α lath width.

In contemporaneous NEWAM research [7, 8], Syed et al consider higher deposition rate WAAM processes. In [7], in the as built condition, typical microstructure of WAAM Ti64 consists of multivariant α colonies forming in the matrix (a basketweave microstructure) and single variant α colonies. Depending on the build strategy, which influences the cooling rate, large microstructure heterogeneity is observed in WAAM built Ti64. Lower cooling rates resulted in larger α lath widths and its colony size. The majority of the β grain boundaries had a continuous α grain boundary (α_{GB}) layer and outward growing single variant α colonies. However, some boundaries that may have had lower misorientation did not have a well-defined α_{GB} layer. Columnar primary β grains resulted in 40% lower elongation in the samples loaded normal to α_{GB} facilitating a preferential path for local damage accumulation along the grain boundary. In conclusion, the formation of such microstructure heterogeneity along the α_{GB} has been shown to influence material performance when subjected to directional cyclic loading.

In later work [8] Syed et al found fatigue performance anisotropy when studying the role of microstructure anisotropy on high cycle fatigue performance of WAAM Ti64 built with different deposition strategies. When the α_{GB} were perpendicular to the applied load, where the majority of the single variant large α colonies are under cyclic loading, this lowered the fatigue performance compared to samples loaded along the α_{GB} .

Fatigue testing.

Despite the progress made, the effect of plasticity on fatigue properties cannot be studied by displacement-, load- or stress-controlled fatigue tests. This is especially the case for the Ti64 alloy as it has little strain hardening capability after yield. Therefore, considering the practical applications, in which stress concentration is unavoidable for structural joints and cut-outs, it is critical to have a comprehensive understanding of the role of microstructure on plasticity to exploit the full potential of WAAM Ti64 under cyclic loading.

Strain controlled fatigue testing will provide insights into the applied elastic-plastic strain energy that drives plasticity leading to fatigue failure. Accurate local strain measurement within the gauge length allows considerably greater precision to be achieved for the strain energy in the low-cycle plastic deformation region. The effect of plasticity is therefore included in the resulting strain vs life fatigue curve, whereas plasticity cannot be determined by load-controlled fatigue testing so is excluded from a resulting stress vs life fatigue curve.

Strain controlled fatigue testing allows a more rigorous and reproducible definition of failure than in load-controlled testing. During strain controlled and load controlled fatigue testing the number of cycles to separation failure is automatically recorded by the test rig controller. However, cycles to separation is not the most appropriate failure criteria to use to identify the number of cycles to failure to use in the strain-life fatigue damage model. During strain controlled fatigue testing, the load varies to maintain the desired cyclic strain amplitude in the gauge length. The material is considered to have failed when the load required to create this strain drops by a given percentage, typically 20% load drop. At the percentage load drop, the number of cycles is recorded, with corresponding load and strain, from which the elastic strain and plastic strain components at failure can be calculated. This drop in load is explained by the presence of a crack, or by a material which has become entirely plastic in its behaviour.

This percentage load drop failure criterion assumes that components made from this material which have lost this percentage of their strength are unlikely to perform as intended and have increased risk of imminent failure.

Strain controlled fatigue testing characterises fatigue performance of a material by testing multiple fatigue specimens at several different total strain ranges to establish a strain-life curve; plotting strain ' ϵ ' against the cycles to failure ' N '. This enables the strain-life curve, and consequent strain-life damage model, to be valid in both the low cycle fatigue (LCF) region where plasticity dominates and the high cycle fatigue (HCF) region where elasticity dominates. Thus, a single and consistent fatigue test method can characterise the material fatigue performance through a wide range of number of cycles to failure, typically between 1×10^2 to 1×10^8 cycles. Most commonly these fatigue tests are conducted fully reversed, with applied strain ratio $R = -1$, and zero initial mean stress. This provides a baseline for analytical mean stress correction methods for fatigue cycles, identified by Rainflow cycle counting, at different R-ratios occurring in variable amplitude load spectra in real world loading conditions. The resulting strain-life fatigue curves are based on material local strain, so they are better suited to analytical predictive methods using local stress or strain values as calculated by finite element analysis. This is in preference to using stress-life fatigue curves which are based on nominal (applied) stresses and are limited in validity to stresses in the elastic region where there is a linear relationship with strain.

MATERIALS AND EXPERIMENTAL METHODS

Materials manufacturing.

Titanium alloy material was deposited on a substrate by wire-arc additive manufacturing (WAAM) using a plasma arc energy source in an inert argon atmosphere using 1.2 mm diameter high quality Ti-6Al-4V wire. The material was deposited using a continuous torch path in a parallel square oscillation pattern across the wall thickness direction (TD), and back-and-forth along the wall longitudinal direction (WD). Two walls were deposited with dimensions of length (L) x height (h) x thickness (t) of 500 mm x 150 mm x 20 mm, using a 5-6 mm/s torch travel speed and 40-45 mm/s wire feed rate with a 60-66% overlap between adjacent melt tracks. Shown schematically in Figure 1.

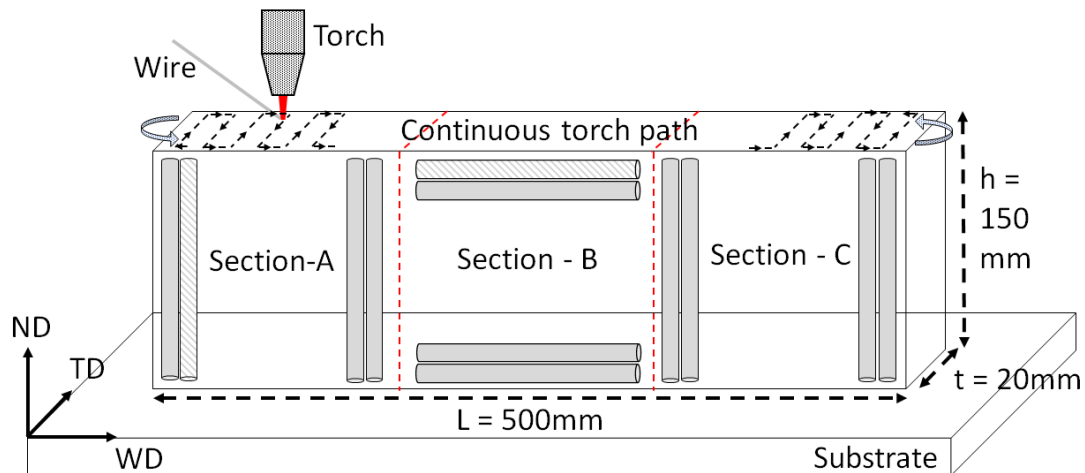


Figure 1: Wall deposition with continuous torch path oscillation across and along the wall, with wall sections for vertical and horizontal sample blank extraction.
(WD – heat source travel direction in the wall longitudinal direction,
TD – wall thickness direction, ND – wall build direction, normal to deposition layers)

Microstructure, texture and micro-XCT analysis.

Test samples for scanning electron microscope (SEM) microstructure analysis and electron back scatter diffraction (EBSD) texture analysis, were extracted in various locations from the TD-ND plane. Test samples for α lath width measurements were extracted from the WD-ND plane at the midpoint of each

wall. Prior to mechanical testing, randomly selected polished fatigue test specimens were examined using micro X-ray computed tomography (micro-XCT). These analyses and their test specifications are described in detail in [3].

Tensile and fatigue test samples manufacture and preparation.

To obtain the maximum number of test samples from the 2 walls, each wall was divided into 3 sections, A, B and C, with cuboid blanks extracted from these in:

- horizontal orientation (Section B in Figure 1) parallel to the deposition plane, where the loading axis is parallel to the deposited layers. This loading axis is perpendicular across the columnar β grains and α grain boundary.
- vertical orientation (Section A and C in Figure 1) normal to the deposition plane, where the loading axis is perpendicular to the deposited layers. This loading axis is parallel along the columnar β grains and α grain boundary.

To ensure a mixture of test sample location from both walls, 31 vertical orientation blanks were extracted from section A and C of wall #1 (x20), and section B of wall #2 (x11), and 31 horizontal orientation blanks from section B of wall #1 (x9), and section A and C of wall #2 (x22). To uniquely identify their original location all blanks were labelled according to their wall number “W1” or “W2”, orientation “H” or “V” and number in the wall “1 to 22”, for example “W1H16”. For each orientation 4 tensile samples and 27 fatigue samples were machined from these blanks. The tensile samples geometry were according to ASTM E8 standard with 5.75 mm gauge diameter and 31.0 mm gauge length. The fatigue samples geometry were according to ASTM E606 standard with 5.0 mm gauge diameter and 10.0 mm gauge length.

The fatigue samples were polished prior to testing to remove any surface imperfections from machining that could act as undesirable fatigue crack initiation sites. The tensile samples were not polished as the surface finish from machining is sufficient and is known not to have an effect on the tensile properties. The fatigue samples were polished to achieve a minimum specification of $R_a=0.2$ in accordance with BS7270 and ASTM E606. Specimens were spot-checked after polishing to ensure the process achieved the required specification.

Tensile tests.

Tensile tests were conducted according to ASTM E8 standard with an applied displacement rate of 1 mm/min, and the strain was measured with a 25 mm gauge length clip-on extensometer (a device for accurate strain measurement). These tests are conducted to check that the material UTS is within expected values, and to determine initial load/strain levels to use for the fatigue tests. Two tests were conducted in ‘as received’ (as machined from the cuboid blank) condition and two in ‘cyclically stabilised’ condition. The cyclically stabilised condition is following 500 sinusoidal strain cycles at an amplitude of 7000 microstrain “ $\mu\epsilon$ ”, this condition is designed to capture the effects of any cyclic hardening/softening on the tensile strength.

Fatigue tests.

Strain controlled fatigue tests were conducted at room temperature with fully reversed (strain ratio $R = -1$) constant amplitude sinusoidal waveforms for cyclic strain amplitude ϵ_a between 4000 to 12000 microstrain “ $\mu\epsilon$ ” (0.004 to 0.012 strain, 0.4% to 1.2 % strain). The strain in the gauge length was measured by a 10 mm gauge length clip-on extensometer and used to control the desired sinusoidal waveform. The test frequency of each fatigue test was varied according to the desired total strain range and material response to maintain the sinusoidal waveform, with test frequencies from 0.25 Hz at the highest cyclic strain amplitude to 5 Hz at the lowest. Failure was defined as the number of cycles when the stress response (calculated from measured load) drops by 20% from the tensile stress magnitude of the half-life stress-strain hysteresis loop. The results from such strain controlled fatigue tests are much more than the number of cycles to failure. These results include high accuracy measurements at high sampling rates (300 samples per second) for strain, load, displacement, cycle number and time.

RESULTS AND DISCUSSION

Microstructure heterogeneity.

The layer wise deposition in AM gives rise to macroscopic heterogeneity of the microstructure in the form of columnar primary β grains aligning in parallel to the build direction. WAAM layer deposition strategies generally produce wider columnar primary β grains compared to other AM processes. This oscillation build strategy produces much wider columnar primary β grains (from 0.43 to 3.0mm) when compared with other WAAM deposition strategies.

Figure 2 shows SEM images in the ND-TD plane of examples of large microstructure heterogeneity, where:

- (a) shows typical transformation bulk microstructure consisting of classical lamellar $\alpha+\beta$ microstructures, with both Widmanstätten multi-variant (basketweave) and single variant colony morphologies.
- (b) shows transformation microstructure along a β grain boundary with continuous grain boundary α colonies. 83% of the primary β grain boundaries studied had a continuous α_{GB} layer with continuous α_{GB} colony with an angle of $\sim 90^\circ$ between neighbouring α lamella growth directions.
- (c) shows transformation microstructure along a β grain boundary with discontinuous α colonies with outwardly growing multi-variant α colonies forming in the matrix (basketweave or Widmanstätten microstructure).

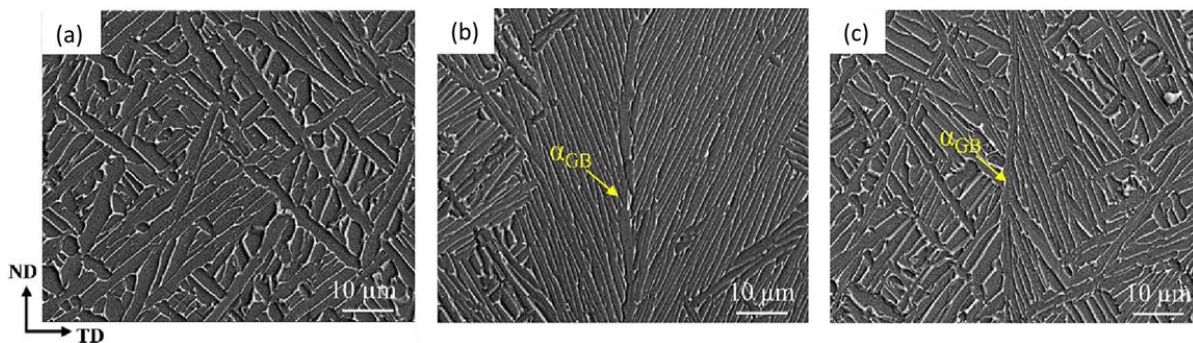


Figure 2: SEM images in the ND-TD plane showing (a) typical transformation bulk microstructure. Transformation microstructure along a β grain boundary with (b) continuous grain boundary α colonies and (c) discontinuous α colonies.

This is a result of the complex cyclic thermal history associated with solidification of sequentially deposited layers, leading to a systematic variation in the $\alpha+\beta$ transformation microstructure. In general, the single variant α colonies extend further into the grains as a result of a much slower cooling rate during the $\beta \rightarrow \beta + \alpha$ transformation with the WAAM process. These single variant α colonies across the α_{GB} indicate a strong crystallographic texture. β grains in WAAM share common neighbouring grains on the crystallographic $[110]_{\beta}$ plane which exclusively lead to the nucleation of continuous α_{GB} colonies either side of the primary β grain boundaries. Some prior β grain boundaries are also decorated with a mixture of multivariant and single variant α colonies on either side, as is typical solidification for AM processes.

Figure 3 shows EBSD maps in the ND-TD plane, along the primary β grain, where:

- (a) shows α phase with continuous α_{GB} colonies (the thick 'pink' region), again indicating a strong crystallographic texture with similar orientation either side of the grain boundary. In Ti64, single variant α_{GB} colonies will develop discontinuously with larger α lamellae nucleating first at lower undercooling (aka. supercooling). These single variant orientation along segments of β grain boundaries grow out rapidly and form skeletal variant templates from which the subsequent continuous α_{GB} colonies develop as the temperature falls and $\beta \rightarrow \beta + \alpha$ transformation progresses.

- (b) shows α phase without continuous α_{GB} colonies (aka. multi-variant α_{GB} colonies) indicating a random or weak crystallographic texture. β grain boundaries without continuous α_{GB} colonies can be seen to have nucleated numerous α orientations, none of which cross the primary β grain boundaries into the neighbouring grains. The α lamellae in the prior β grain interiors largely have a typical basketweave morphology with a high aspect ratio.

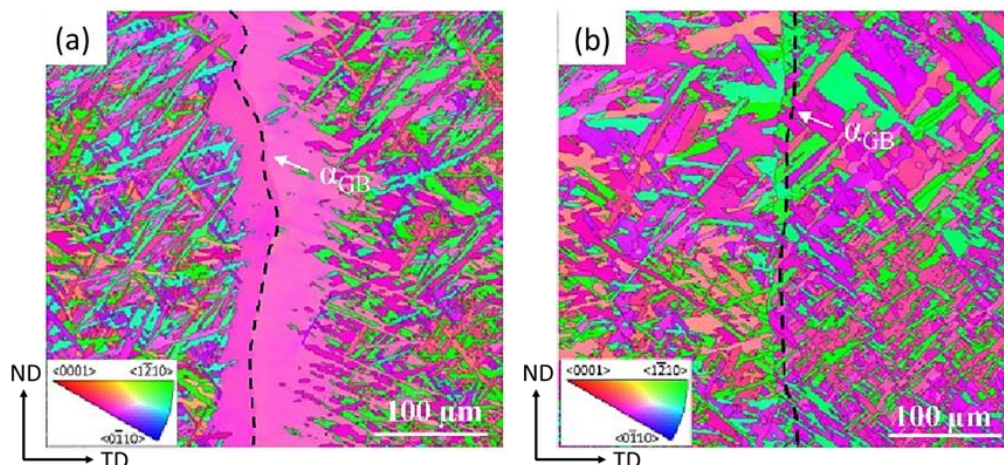


Figure 3: EBSD maps in the ND-TD plane, along the primary β grain, showing α phase (a) with and (b) without continuous grain boundary α colonies.

This microstructure heterogeneity is described in considerably more detail in [3].

Micro-XCT analysis.

Figure 4 shows the micro XCT analysis results showing no porosity in the gauge length of a fatigue test sample (a) by 3D rendering of a helix scan with 60% transparency and (b) by cone beam orthogonal slice. The sample has been found very homogeneous showing no sign of defects or porosity down to the $\sim 7.4\text{mm}$ resolution limit. This homogeneity is illustrated by the absence of any features in the 3D rendering of the helix scan and similar absence of any features in the ‘grey’ cone beam orthogonal slice of which this is just one slice from a video sequence of continuous orthogonal slices through the gauge length.

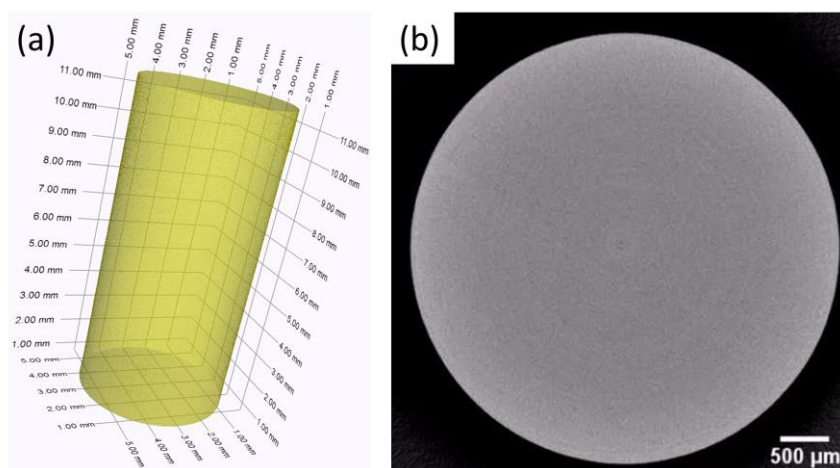


Figure 4: Micro XCT analysis results showing no porosity in the gauge length of a fatigue test sample (a) by 3D rendering of a helix scan with 60% transparency and (b) by cone beam orthogonal slice.

Tensile properties

Tensile properties obtained from the engineering stress–strain of the tensile test measurements are presented in Table 1 and compared with conventionally manufactured Ti64 and minimum tensile properties recommended for PBF AM Ti64:

- Ti64 specification AMS 4928, wrought bar, annealed (12.7 mm thickness), from MMPDS [9]
- Ti64 specification AMS 4992, cast, HIPed and annealed (< 12.7 mm thickness) [9]
- Ti64 specification ASTM F2924 for additive manufacturing Ti64 with powder bed fusion [10]

Table 1: Tensile properties of Ti-6Al-4V obtained from the engineering stress–strain data.

Material property	WAAM Horizontal	WAAM Vertical	Wrought (AMS 4928)	Cast (AMS 4992)	ASTM F2924
Yield strength (YS _{0.2}), MPa	842 ± 14	800 ± 23	861	765	825
Ultimate tensile strength (UTS), MPa	951 ± 12	898 ± 24	930	861	895
Elongation (%)	11 ± 2	17 ± 5	10 *	5	10

* AMS 4928 Elongation = 10% from MMPDS-11 [9], is stated as 25% in [3] from MMPDS-04.

WAAM Ti64 tensile strengths are comparable with their wrought counterpart and higher than the cast material. Horizontal orientation samples exceed the ASTM F2924 minimum tensile property requirements, whilst the vertical samples are equal to or just below these minimum requirements. Horizontal orientation samples showed higher yield and tensile strengths compared to the vertical samples, whereas higher elongation was found in the vertical samples. This higher elongation in vertical samples is the result of a combined effect of the bulk microstructure (α lath size) and α_{GB} parallel to the loading axis which has contributed to the plastic deformation, thereby increased ductility.

This anisotropy in ductility is generally observed in AM built Ti64 and is linked to the epitaxially grown primary β grains. It has been shown that α variant greatly influence the mechanical properties in AM Ti64. Material with single variant α colonies shows a stronger crystallographic texture which increases the effective slip length and allows the dislocations to move freely within the colonies during the tensile deformation. Syed et al continue this discussion in [3].

Cyclic deformation behaviour

Under cyclic loading, material damage is progressive and develops as a consequence of dislocations, rearrangement and persistent slip bands leading to localised plastic deformation. The cyclic response of materials depends on the test conditions, microstructure and its constituents that are influenced by their processing route. In the case of AM built materials, sample orientation plays a major role in the cyclic deformation and damage mechanisms. Amongst these, the effect of sample orientation and applied strain amplitudes are the two variables investigated in this study. This analysis of the cyclic deformation behaviour uses the strain, load and cycle number measurements from the strain controlled fatigue tests, where the high sampling rate provides many high accuracy measurement points for every fatigue cycle.

Figure 5 shows the progression of maximum cyclic stress versus normalised load cycles, N/N_f , where N is the cycle number and N_f is the number of cycles to fatigue separation failure:

- (a) shows a schematic of maximum cyclic stress vs normalised load cycles illustrating three distinct stages of the cyclic stress response under strain controlled fatigue test.
 - Stage 1 represents a rapid cyclic softening where a steep decrease in applied stress is observed, for about 5–15% of total fatigue lifetime.
 - Stage 2 represents a progressive quasi-stable cyclic response with a noticeable and continuous cyclic softening where a gradual decrease in applied stress is observed, for about 75-80% of total fatigue lifetime.
 - Stage 3 is the final stage governed by rapid fatigue crack propagation leading to failure, where a rapid decrease in applied stress is observed, for 0-5% of total fatigue lifetime. This stage is the reason why a number of cycles to a % load drop failure criteria is commonly used in preference to the number of cycles to separation.

- The variation of percentage of total fatigue lifetime in each stage depends on the material response to the magnitude of the cyclic strain amplitude of the strain controlled fatigue test and consequent calculated applied stress as the measured load changes.
- (b) shows the progression of maximum cyclic stress versus normalised load cycles for the horizontal orientation fatigue test samples. In this horizontal orientation the loading axis is parallel to the deposited layers, so is loaded across columnar β grains and α_{GB} . In general, cyclic softening is apparent in both this horizontal and vertical (not shown) orientation under different strain amplitudes (ϵ_a) except when elastic deformation is dominant, $\epsilon_a \leq 0.6\%$ strain. The three distinct stages are observed when applied strain amplitudes $\epsilon_a > 0.6\%$ strain where the total strain includes an elastic and a plastic strain component. The absence of Stage 1 when applied strain amplitudes $\epsilon_a \leq 0.6\%$ strain is because the total strain is entirely, or almost entirely, elastic.
- (c) shows that the cyclic softening rate for both horizontal and vertical orientations is similar at lower strain amplitudes, $\epsilon_a \leq 0.6\%$ strain where elasticity dominates. Above this, for cyclic strain amplitudes $\epsilon_a \geq 0.7\%$ the cyclic softening rate increases dramatically in both orientations and stabilises with a plateau response. In this region the cyclic softening rate for vertical orientation is approximately 2x higher than the horizontal at the same cyclic strain amplitude.

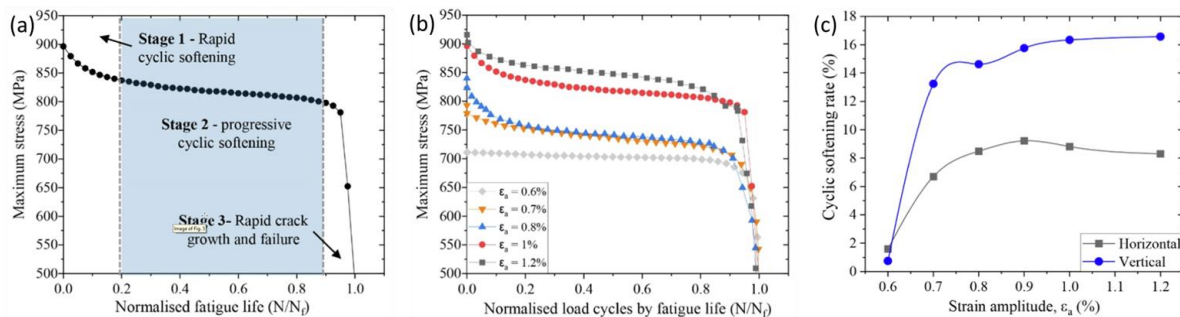


Figure 5: (a) Three stages of maximum cyclic stress vs normalised fatigue life
 (b) Maximum cyclic stress vs normalised fatigue life for horizontal orientation fatigue tests,
 (c) Cyclic softening rate under different cyclic strain amplitudes.

This difference in cyclic softening rate in Figure 5 (c) for horizontal and vertical orientation fatigue samples, together with the EBSD results in Figure 3, confirm that the cyclic stress response and resulting fatigue damage accumulation is influenced by sample orientation microstructure heterogeneity resulting in property anisotropy in WAAM built Ti64.

In [3] Syed et al continue this review of cyclic deformation behaviour with discussion of:

- Comparison of cyclic softening at the same strain amplitude $\epsilon_a = 1.0\%$ strain of WAAM built Ti64 with laser beam and electron beam PBF built Ti64 and wrought Ti64. WAAM built Ti64 shows similar cyclic softening behaviour to electron beam PBF and wrought built Ti64 because all these processes result in fully transformed $\alpha + \beta$ with Widmanstätten and colony morphologies.
- Examination of differences in tension-going (loading) and compression-going (unloading) elastic modulus. Under strain-controlled fatigue testing reduction in the elastic modulus can be observed in the loading and unloading excursions. In general the elastic modulus when the sample is in tension during the first part of the compression excursion is less than the modulus when the sample is under compression in the first part of the compression excursion due to the difference in the microcracks or defects being open or closed. This difference between the apparent elastic moduli in compression and tension becomes larger as more microcracks initiate and propagate.

Fatigue test results

Figure 6 shows an example of measurement post-processing for each fatigue test where:

- (a) shows the maximum and minimum strain for every fatigue test cycle, showing the constant strain control, and the stress calculated from the slowly and then rapidly reducing load.

- (b) shows stress-strain hysteresis loops for 3 selected cycles, an early life stable loop after soft-start, the half-life stable loop (used to define the % load drop levels, and for cyclic stress-strain curves) and the failure loop for the chosen % load drop failure criteria.
- (c) shows the cycle number, total stress range (MPa), total strain range ($\mu\epsilon$) and elastic and plastic strain components of the hysteresis loops shown in (b).
- (d) shows additional fatigue test details, including cycles to separation, cycles to % load drops, cycle rate, cross sectional area and waveform.

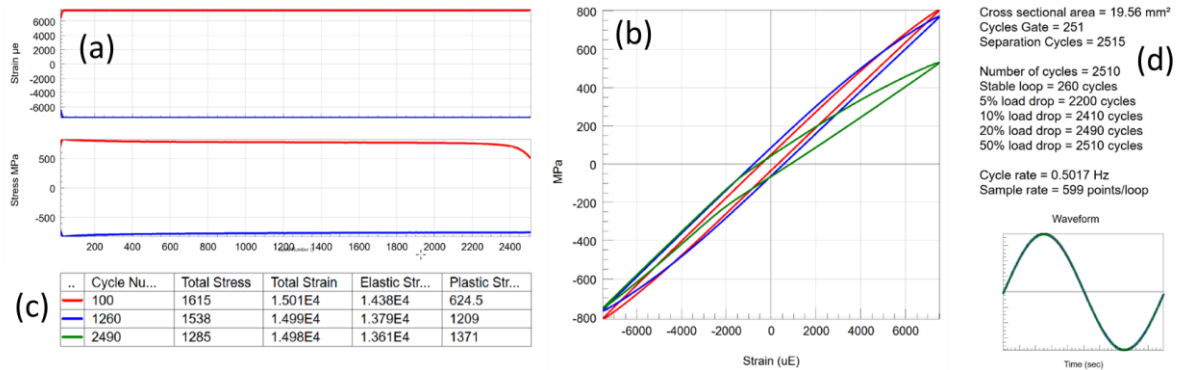


Figure 6: (a) strain ($\mu\epsilon$) and stress (MPa) vs cycle number, (b) stress-strain hysteresis loops, (c) hysteresis loops results table, and (d) additional fatigue test details

Figure 7 (a) shows strain vs fatigue life test results from the WAAM Ti64 horizontal and vertical samples. For comparison this includes fatigue test results from literature for polished fatigue samples from equivalent Ti64 material manufactured by different processes:

- by mill annealed wrought hot rolled bar, with extra low interstitials [11]
- by laser beam PBF in as built condition [12]
- by laser blown powder DED in as built condition [13]

WAAM Ti64 showed generally lower fatigue life than the mill annealed in the LCF regime and in transition to HCF regime. When cyclic strain amplitude $\epsilon_a > 0.6\%$ strain, WAAM horizontal and vertical samples showed an average of 5.7 and 2.2 times lower fatigue life compared to wrought mill annealed material. Plastic deformation in titanium alloys is accommodated by a complex mixture of crystallographic slip and deformation twinning. As a result, when cyclic strain amplitude $\epsilon_a > 0.6\%$ strain, where plasticity dominates the fatigue life through crack closure, WAAM samples showed lower fatigue life. When $\epsilon_a < 0.6\%$ strain, where the applied stresses are within the elastic regime, i.e., no influence of plasticity, WAAM showed similar fatigue properties as wrought Ti64. Though comparison is limited in this part of the HCF regime due to the lack of comparative fatigue test results for ϵ_a between 0.4 and 0.6% strain for wrought mill annealed material.

Figure 7 (b) shows the monotonic stress-strain curve from the tensile tests and compares these with the cyclic stress-strain curves. These cyclic stress-strain curves are obtained by connecting the tips of the half-life stabilised cyclic hysteresis loops for each of the applied cyclic strain amplitudes. This confirms that WAAM Ti64 material in both horizontal and vertical orientation exhibit a small amount of cyclic softening behaviour. At a given strain value beyond the yield point, the vertical orientation samples show lower stress indicating higher ductility in this vertical orientation. This corresponds with the higher elongation tensile property, from 11% in horizontal orientation to 17% in vertical orientation, shown in Table 1.

The derivation of strain-life fatigue properties is by separating the total strain range of the half-life hysteresis loops into their elastic and plastic terms according to the Basquin and Coffin-Manson equations respectively, and subsequent curve fitting. Figure 8 shows regression curve fitting for mean fatigue life for these WAAM Ti64 (a) horizontal and (b) vertical fatigue test results. Syed et al describe fitting these results in detail in [3].

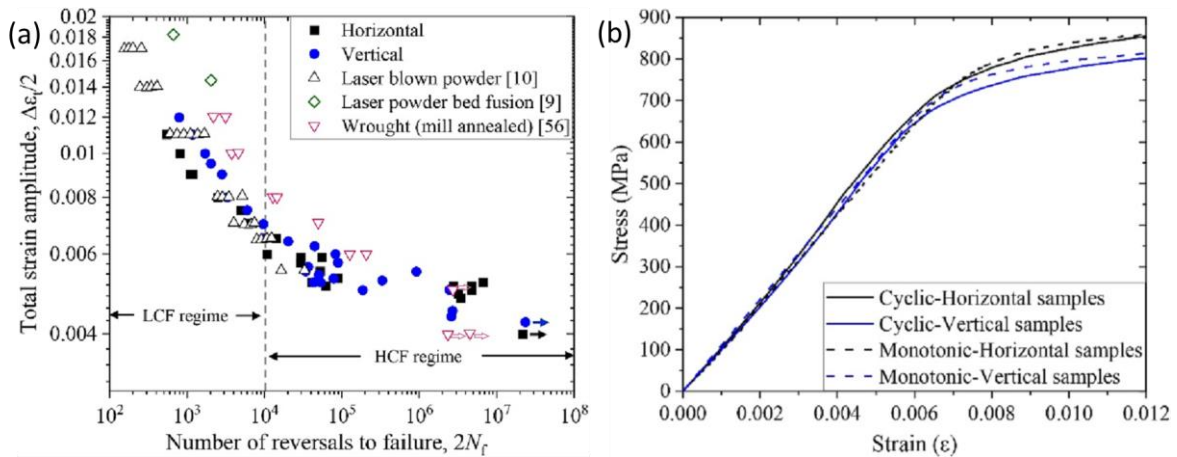


Figure 7: (a) strain vs fatigue life test results for WAAM Ti64 samples and literature data (b) cyclic and monotonic stress–strain curves.

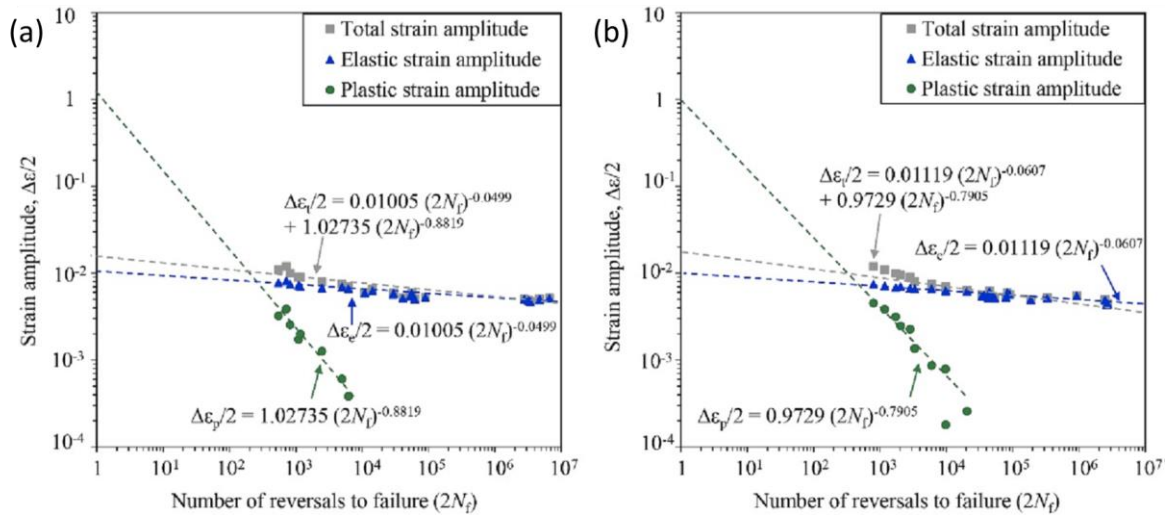


Figure 8: Fitting lines of the fatigue tests by their total strain, elastic strain (Basquin equation), and plastic strain (Coffin-Manson equation) for (a) horizontal and (b) vertical samples

Fractography

The fractured samples were analysed using scanning electron microscope (SEM) to identify the fatigue crack initiation sites. All of the failed fatigue test samples were inspected (this excludes the test runouts at fatigue life > 10⁷ cycles) and amongst all of these samples, 96% had crack initiation from the α phase, of which 66% at the surface and 30% near the surface. Crack initiation is mainly dominated by the type of microstructure (lamellar or bi-modal), α-lamellae width and associated crystallographic texture. Under cyclic loading, crack nucleation in α + β titanium alloys is attributed to the occurrence of heterogeneous deformation in the form of intense slip bands within the α phase or at α_{GB} along prior β grain. The microstructure in WAAM Ti64 consists of the Widmanstätten and colony morphology.

Figure 9 shows representative SEM fractography where:

- (a) and (b) show regions of crack initiation, propagation and final failure. No defects were found in the fracture faces of any of the samples confirming the material is fully dense. Crack initiation sites in the fracture faces were either from α or α/β lamellar interface.
- (c) an example of a secondary crack, all the samples showed several secondary cracks in various directions with respect to the primary crack growth direction. In general terms, the oscillation build strategy has resulted in large and more defined single variant α colonies. The propagation of secondary cracks is the result of micro crack deflection at short length scale that is more characteristic of the size of multivariant colonies found within the coarse β grains.

- (d), (e) and (f) show the fracture surface features in the fatigue crack propagation regions at different strain amplitudes. The crack propagation features are similar in both sample orientations at the same strain amplitudes. Samples tested at different strain amplitude exhibit different fatigue features, those at (i) higher strain amplitudes (1.2% strain) show ductile fracture features, indicating a damage mechanism governed by plastic deformation, and at (ii) lower strain amplitudes (0.8% and 0.6% strain) show the classic striation marks on the fracture surface indicating slow or incremental growth of a fatigue crack. The insets in (e) and (f) show wider striation at 0.8% than at 0.6% strain indicating higher crack growth rate and shorter fatigue life for the former.

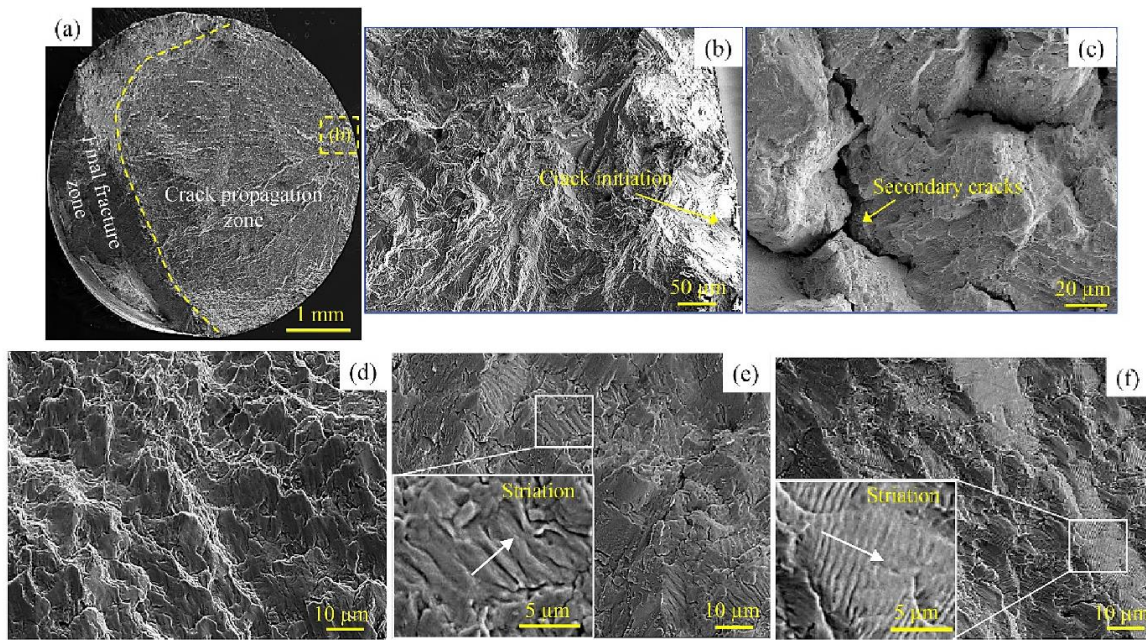


Figure 9: SEM fractography images (a) overview of the fracture surface, (b) crack initiation from a microstructure feature, (c) secondary cracks found in the crack propagation region. Fracture surfaces of samples at different strain amplitudes ϵ_a : (d) 1.2%, (e) 0.8%, (f) 0.6% strain. Inset figures in (e) and (f) show striation marks from crack growth.

CONCLUSIONS

Cyclic deformation and fatigue behaviour of a WAAM Ti64 alloy were investigated by strain-controlled fatigue test to study the influences of sample orientation and microstructure characteristics. Tensile properties were also measured as part of the study. Based on the experimental findings and analysis, the following conclusions can be drawn:

1. Slower cooling rates associated with the oscillation build strategy have resulted in large single variant α colonies with strong crystallographic texture along the primary columnar β grain boundaries.
2. Between the two sample orientations, tensile and yield strengths are 5% higher normal to the material build direction (horizontal samples) owing to the columnar primary β grains with strong crystallographic texture along the α_{GB} that is perpendicular to the loading axis.
3. Between the two sample orientations, elongation is 50% higher in the material build direction (vertical samples) owing to the combined effect of the bulk microstructure (α lath size) and α_{GB} parallel to the loading axis increasing ductility.
4. Cyclic stress softening is observed in both sample orientations when the applied strain amplitude exceeds 0.6% strain. Because of higher ductility, the cyclic softening rate in vertical samples is approximately two times higher when strain amplitude is higher than 0.7% strain. As a result, horizontal samples show slightly higher peak stress by up to 4% compared to the vertical samples.

5. In the low cycle fatigue regime ($2N_f < 10^4$ load reversals), the vertical samples' average life is about 2.5 times longer than that of the horizontal samples due to higher ductility in the former. In the high cycle fatigue regime ($2N_f > 10^4$), fatigue life performance is almost isotropic.
6. SEM fractography has confirmed no porosity defects in the material as per the micro-XCT result and revealed the fatigue crack initiation sources being either the α laths or α/β interface due to cyclic slip localisation. All samples have shown secondary cracks because of micro cracks deflection at short length scales in various directions with respect to the primary crack growth plane, due to the presence of large and more defined single variant α colonies. Such crack deviation has contributed to achieving longer fatigue life.

REFERENCES

- [1] “New Wire Additive Manufacturing (NEWAM)”, UK Engineering and Physical Sciences Research Council (EPSRC), <https://gow.epsrc.ukri.org/NGBOViewGrant.aspx?GrantRef=EP/R027218/1>.
- [2] “New Wire Additive Manufacturing (NEWAM)”, UK Research and Innovation (UKRI), <https://gtr.ukri.org/projects?ref=EP%2fR027218%2f1>.
- [3] Syed, A. K., Plaskitt, R., Hill, M., Pinter, Z., Ding, J., Zboray, R., Williams, S., Zhang, X. (2023), *Strain controlled fatigue behaviour of a wire + arc additive manufactured Ti-6Al-4V*, Int J Fatigue 2023;171:107579, <https://www.sciencedirect.com/science/article/pii/S0142112323000804>.
- [4] Syed, A. K., Hill, M., Plaskitt, R., Zhang, X. (2021), *Cyclic deformation and fatigue behaviour of titanium alloy Ti-6Al-4V built by directed energy deposition AM process*, Video proceedings of 2nd European Conference on the Structural Integrity of Additively Manufactured Materials (ESIAM21), <https://doi.org/10.53254/ESISTUBE.ESIAM21.32>.
- [5] Williams, S., Zhang, X., Plaskitt, R., Syed, A. K. (2021), *Wire-Arc Additive Manufacturing*, Video proceedings of HBK Technology Days, <https://www.hbkworld.com/en/knowledge/events/2021-hbk-technology-days#day2>.
- [6] New Wire Additive Manufacturing, NEWAM, website <https://newam.uk/>, and research papers <https://newam.uk/documents/research-papers/view>.
- [7] Syed AK, Zhang X, Davis AE, Kennedy JR, Martina F, Ding J, et al. *Effect of deposition strategies on fatigue crack growth behaviour of wire + arc additive manufactured titanium alloy Ti-6Al-4V*, Mater Sci Eng A 2021;814:141194. <https://doi.org/10.1016/j.msea.2021.141194>.
- [8] Syed AK, Zhang X, Caballero A, Shamir M, Williams S., *Influence of deposition strategies on tensile and fatigue properties in a wire + arc additive manufactured Ti-6Al-4V*, Int J Fatigue 2021;149:106268. <https://doi.org/10.1016/j.ijfatigue.2021.106268>.
- [9] Metallic Materials Properties Development and Standardization (MMPDS-11), 2016.
- [10] ASTM F2924-14, Standard Specification for Additive Manufacturing Titanium-6, Aluminum-4 Vanadium with Powder Bed Fusion, in: ASTM Int., West Conshohocken, PA, 2014.
- [11] Carrion. P. E., Shamsaei, N., Daniewicz, S. R., Moser, R. D., *Fatigue behaviour of Ti-6Al-4V, ELI including mean stress effects*, Int J Fatigue 2017;99:87–100. <https://doi.org/10.1016/j.ijfatigue.2017.02.013>.
- [12] Agius, D., Kourousis, K. I., Wallbrink, C., Song, T., *Cyclic plasticity and microstructure of as-built SLM Ti-6Al-4V: The effect of build orientation*, Mater Sci Eng A 2017;701:85–100, <https://doi.org/10.1016/j.msea.2017.06.069>.
- [13] Ren, Y. M., Lin, X., Guo, P. F., Yang, H. O., Tan, H., Chen, J., et al, *Low cycle fatigue properties of Ti-6Al-4V alloy fabricated by high-power laser directed energy deposition: Experimental and prediction*, Int J Fatigue 2019;127:58–73. <https://doi.org/10.1016/j.ijfatigue.2019.05.035>.